Inorg. Chem. **2005**, *44*, 3449–3458

Inorganic Chemistry Article

Silylchalcogenolates $MESiR^tBu_2$ (M = Na, Cu, Zn, Fe; E = S, Se, Te; R = ^tBu, Ph) and Disilyldichalcogenides $^tBu_2RSiE–ESiR^tBu_2$ (E = S, Se, Te; R = ^tBu, Ph): Synthesis, Properties, and Structures

Theresa I. Kückmann, Melina Hermsen, Michael Bolte, Matthias Wagner, and Hans-Wolfram Lerner*

Institut für Anorganische Chemie, Johann Wolfgang Goethe–Universität Frankfurt am Main, Marie-Curie-Strasse 11, 60439 Frankfurt am Main, Germany

Received September 15, 2004

The sodium silyl chalcogenolates $NaESiR^tBu_2$ (R = Ph, ^tBu; E = S, Se, Te), accessible by the nucleophilic degradation of S, Se, or Te by the sodium silanides $NaSiR^tBu_2$ (R = Ph, ^tBu), have been characterized by X-ray structure analysis. Protonolysis of the sodium silyl chalcogenolates yields the corresponding chalcogenols. The Cu and Zn chalcogenolates, $[Cu(SSiPh^tBu_2)]_4$ and $[ZnCl(SSi^tBu_3)(THF)]_2$, have been synthesized by metathesis reactions of CuCl with $NaSSiPh^tBu_2$ and of $ZnCl_2$ with $NaSSi^tBu_3$, respectively. The solid-state structures of the transition metal thiolates have been determined. The compounds $^tBu_2RSiE–ESiR^tBu_2$ (R = Ph, ^tBu; E = S, Se, Te) are accessible via air oxidation. With the exception of $^tBu_3SiS–SSi^tBu_3$, these compounds were analyzed using X-ray crystallography and represent the first structurally characterized silylated heavy dichalcogenides. Oxidative addition of $^tBu_3SiTe–TeSi^tBu_3$ to $Fe(CO)_5$ yields $[Fe(TeSi^tBu_3)(CO)_3]_2$, which has also been structurally characterized.

Introduction

In a number of recent studies, bulky silyl chalcogenolate ligands of the type R_3SiE^- (E = O, S, Se, Te) have been used to stabilize transition metal centers. Such ligands have drawn interest for a number of reasons. The chalcogen donor atoms are often found to bridge metal centers, suggesting possible applications in the stabilization of transition metal clusters.[1] At the same time, the large organic substituents, such as phenyl, *tert*-butyl, and trimethylsilyl, with or without bulky ancillary ligands, control the nuclearity of the compounds, sometimes even producing mononuclear complexes.[2] The resulting low nuclearity and increased solubility make such compounds easier to characterize and study. Investigations of the reactivity of the supersilyl group ($^tBu_3Si^-$), including preliminary studies of its reactivity with chalcogens, have been reported.[3] It has also been suggested that bulky siloxides can function as analogues for the ubiquitous cyclopentadienyl (Cp) ligand.[4] These sterically hindered ligands enforce a nearly linear Si–O–M coordination angle, allowing for π donation from the oxygen atom to the metal center. This makes such siloxides formal five-electron donors, whereas the large substituents lead to a cone angle that approaches that of the Cp ring. Obviously, the heavier chalcogens will behave differently than oxygen. They are generally regarded as better electron donors, but their large size makes the enforcement of linear coordination, which is necessary for π donation, more difficult. Further investigation is needed to better understand these effects.

Here, we present the synthesis and characterization of the bulky silyl chalcogenolate ligands $^tBu_2RSiE^-$ (R = Ph, ^tBu; E = S, Se, Te). These compounds display interesting redox behavior, and initial investigations of their coordination chemistry with first-row transition metals make them interesting candidates for the development of low nuclearity, potentially redox-active metal clusters. In addition, the simultaneous investigation of the chalcogen elements in the third through fifth periods gives us the opportunity to compare their reactivity and to decipher trends in their coordination behavior.

* Author to whom correspondence should be addressed. Fax: +49-69798-29260. E-mail: lerner@chemie.uni-frankfurt.de.

(1) (a) Sydora, O. L.; Wolczanski, P. T.; Lobkovsky, E. B. *Angew. Chem.* **2003**, *115*, 2789. (b) Komuro, T.; Matsuo, T.; Kawaguchi, H.; Tatsumi, K. *J. Chem. Soc., Dalton Trans.* **2004**, 1618. (c) Komuro, T.; Kawaguchi, H.; Tatsumi, K. *Inorg. Chem.* **2002**, *41*, 5083.
(2) (a) Gindelberger, D. E.; Arnold, J. *Inorg. Chem.* **1993**, *32*, 5813. (b) Tran, D. T. T.; Corrigan, J. F. *Organometallics* **2000**, *19*, 5202. (c) Chownacki, J.; Becker, B.; Konitz, A.; Potrzebowski, M. J.; Wojnowski, W. *J. Chem. Soc., Dalton Trans.* **1999**, 3063.
(3) Wiberg, N. *Coord. Chem. Rev.* **1997**, *163*, 217.
(4) Wolczanski, P. T. *Polyhedron* **1995**, *14*, 3335.

10.1021/ic048710j CCC: $30.25 © 2005 American Chemical Society
Published on Web 04/07/2005

Results and Discussion

Synthesis. Despite significant interest in alkyl and aryl silyl chalcogenolates as ligands for transition metal centers, no single method of their preparation has established itself as the most advantageous. In some instances, the corresponding chalcogenols have been deprotonated in situ by acidic metal centers.[1c,2a] In others, disilyl chalcogenides have been employed in substitution reactions with metal halides, leading to the thermodynamically favorable release of Me_3SiX and the coordination of an R_3SiE ligand to the metal center.[2b] In a different approach, lithium silylthiolates of the type $LiSSiRMe_2$ were prepared by cleavage of cyclotrisilathiane $(Me_2SiS)_3$ with methyllithium or *tert*-butyllithium.[1b] The applicability of these methods, however, is limited by the availability of suitable precursors. The bulky organic substituents of our target molecules, for instance, make the synthesis of corresponding cylcosilathianes impractical, and of the chalcogenols relevant to the targeted ligands, only $^tBu_3SiSH$ is known.[3] For these reasons, a more general synthetic route was applied. This method, previously described by Arnold and co-workers for a number of related compounds,[5] involves the insertion of elemental chalcogen into the silyl−alkali metal bond of precursor alkali silanides. In this case, the sodium silanides $NaSiR^tBu_2$ (R = Ph, ^{t}Bu), accessible by reduction of halosilane precursors, are converted to the corresponding sodium silyl chalcogenolates, as shown in eq 1.

$$NaSiR^tBu_2 + E \rightarrow \begin{array}{c} NaESiR^tBu_2 \\ \textbf{1a}:\ E = S, R = Ph \\ \textbf{1b}:\ E = Se, R = Ph \\ \textbf{1c}:\ E = Te, R = Ph \\ \textbf{1d}:\ E = S, R = {}^tBu \\ \textbf{1e}:\ E = Se, R = {}^tBu \\ \textbf{1f}:\ E = Te, R = {}^tBu \end{array} \quad (1)$$

When equimolar amounts of the reactants in THF are used, the products are obtained cleanly with only minor impurities as a result of silanide hydrolysis and oxidation. The product solutions are clear and yellow or orange in donor solvents. Slow solvent evaporation yields off-white crystals, which are readily soluble in polar organic solvents, slightly soluble in aromatic solvents, and sparingly soluble in hydrocarbons.

The sodium chalcogenolates **1a**−**1f** are air-sensitive. Upon standing under atmospheric conditions, they are oxidized to the corresponding disilyldichalcogenides $^tBu_2RSiE{-}ESiR^tBu_2$ (R = Ph, ^{t}Bu; E = S, Se, Te) (see eq 2). This oxidation is accompanied by a color change to brick red for the selenium species and to deep ink blue for the tellurium species; the sulfur species are yellow. Filtration and recrystallization from pentane yields the dichalcogenides in pure, crystalline form. NMR spectroscopy also confirms the symmetric structure of the compounds.

$$2NaESiR^tBu_2 \xrightarrow[-\ Na_2O_2]{+\ O_2} \begin{array}{c} {}^tBu_2RSiE{-}ESiR^tBu_2 \\ \textbf{2a}:\ E = S, R = Ph \\ \textbf{2b}:\ E = Se, R = Ph \\ \textbf{2c}:\ E = Te, R = Ph \\ \textbf{2d}:\ E = S, R = {}^tBu \\ \textbf{2e}:\ E = Se, R = {}^tBu \\ \textbf{2f}:\ E = Te, R = {}^tBu \end{array} \quad (2)$$

Similar behavior has been observed for the hypersilyl species $(THF)_2LiTeSi(SiMe_3)_3$, which can be oxidized to dark green $(Me_3Si)_3SiTeTeSi(SiMe_3)_3$.[5a] The disilyl disulfides, while accessible via air oxidation, can also be synthesized by reaction of the corresponding sodium silanides with S_2Cl_2 in THF, as depicted in eq 3.

$$2NaSiR^tBu_2 + S_2Cl_2 \xrightarrow{-\ 2NaCl} {}^tBu_2RSiS{-}SSiR^tBu_2 \quad R = {}^tBu, Ph \quad (3)$$

Filtration and recrystallization from pentane yields the product disulfides as pale yellow blocks.

The dichalcogenides are stable under atmospheric conditions; the disulfides **2a** and **2d** and diselenides **2b** and **2e** show no signs of decomposition after several weeks of exposure to moist air. Ditelluride **2f** is also stable under atmospheric conditions. Only the less bulky ditelluride **2c** shows signs of hydrolysis from atmospheric water vapor.

Oxidation to the disilyldichalcogenides can, however, be reversed by reduction with alkali metals. When **2f** is exposed to an excess of potassium metal at room temperature, the dark blue color slowly disappears and only those NMR signals corresponding to the silyl chalcogenolate anion are observed (eq 4).

$$^tBu_3SiTe{-}TeSi^tBu_3 + 2K \rightarrow 2KTeSi^tBu_3 \quad (4)$$

When diselenide **2e** in THF is subjected to cyclic voltammetric investigations, an irreversible reduction peak is observed at −1.37 V (vs ferrocene$^{1+/0}$). This is comparable to the reduction of PhSeSePh in acetonitrile, which occurs at −0.85 V versus SCE[6] (−1.23 V vs ferrocene$^{1+/0}$).[7] The reduction of diphenyl diselenide, however, is a reversible, one-electron process. The electrochemical irreversibility of the reduction of **2e** indicates that the Si−Se−Se−Si moiety is less stable than the C_{Ph}−Se−Se−C_{Ph} unit. This observation can be rationalized by considering the positive inductive effects of the Si^tBu_3 substituents, which can be expected to increase the overall electron density in the Si−Se−Se−Si unit, as compared to the negative inductive effects of the phenyl substituents, which should decrease the overall charge density of the C_{Ph}−Se−Se−C_{Ph} moiety.

Under the same experimental conditions, no comparable reduction wave was found for ditelluride **2f**. This result suggests that the reduction potential of **2f** is significantly more negative than that of **2e**, making the ditelluride harder to reduce but the corresponding tellurolate easier to oxidize.

Compounds **1a**−**1f** are also sensitive to protonolysis. When treated with an excess of trifluoroacetic acid in C_6D_6,

(5) (a) Bonasia, P. J.; Gindelberger, D. E.; Dabbousi, B. O.; Arnold, J. *J. Am. Chem. Soc.* **1992**, *114*, 5209. (b) Bonasia, P. J.; Christou, V.; Arnold, J. *J. Am. Chem. Soc.* **1993**, *115*, 6777.

(6) Sobkowiak, A.; Sawyer, D. T. *Inorg. Chem.* **1990**, *29*, 1248.

(7) Conelly, N. G.; Geiger, W. E. *Chem. Rev.* **1996**, *96*, 877−910.

the silyl chalcogenolates are converted into the corresponding silyl chalcogenols ${}^t\mathrm{Bu_2RSiEH}$ (R = Ph, ^{t}Bu; E = S, Se, Te), as shown in eq 5.

$$\mathrm{NaESiR^tBu_2 + CF_3CO_2H \xrightarrow{-\,CF_3CO_2Na} {}^tBu_2RSiEH} \tag{5}$$

3a: E = S, R = Ph
3b: E = Se, R = Ph
3c: E = Te, R = Ph
3d: E = S, R = ^{t}Bu
3e: E = Se, R = ^{t}Bu
3f: E = Te, R = ^{t}Bu

This reaction occurs quantitatively, as determined by ^{1}H NMR spectroscopy, with the signals of the starting material protons disappearing completely. The products are easily identified by the characteristic upfield shift of the chalcogenol protons. The tellurol signals are observed near −7.5 ppm; the selenol and thiol signals are found near −2.5 and −0.5 ppm, respectively. The thiols **3a** and **3d** and selenols **3b** and **3e** are stable in C_6D_6 solution at room temperature for several months. As shown in eq 6, tellurol **3f** slowly oxidizes to ditelluride **2f**.

$$\underset{\mathbf{3f}}{2\,{}^t\mathrm{Bu_3SiTeH}} \xrightarrow[-\,\mathrm{H_2O}]{+\,0.5\mathrm{O_2}} \underset{\mathbf{2f}}{{}^t\mathrm{Bu_3SiTe{-}TeSi}{}^t\mathrm{Bu_3}} \tag{6}$$

As expected, the silyl chalcogenolates proved to be suitable ligands for transition metal complexes. Salt metathesis reactions of the sodium silyl thiolates **1a** and **1d** with CuCl and $ZnCl_2$ in THF produced the transition metal silyl thiolates $[\mathrm{Cu(SSiPh^tBu_2)}]_4$ (**4**) and $[\mathrm{ZnCl(SSi^tBu_3)(THF)}]_2$ (**5**), respectively. After changing the solvent to toluene and removing byproduct salts by filtration, the complexes were obtained in crystalline form. Both compounds **4** and **5** are air-sensitive. Copper thiolate **4** crystallizes as colorless needles, whereas the zinc thiolate **5** is deposited as colorless blocks.

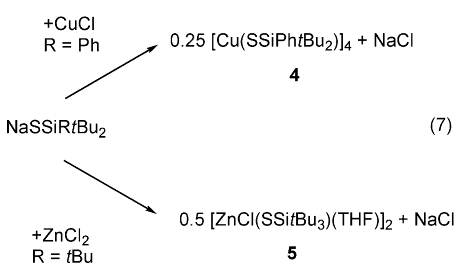

(7)

The oxidative addition of dichalcogenides to low-oxidation-state metals has been established as a common synthetic route,[8] although it has not yet, to our knowledge, been applied with disilyl dichalchogenides. When a 2:1 benzene solution of $Fe(CO)_5$ and **2f** is irradiated with a commonplace fluorescent lamp, a color change from the ink blue of the ditelluride to a deep red is observed, and the dinuclear complex $[\mathrm{Fe(TeSi^tBu_3)(CO)_3}]_2$ is formed cleanly and quantitatively, as determined by NMR spectroscopy. Slow evaporation of the solvent leads to the deposition of red plates suitable for X-ray crystal structure analysis.

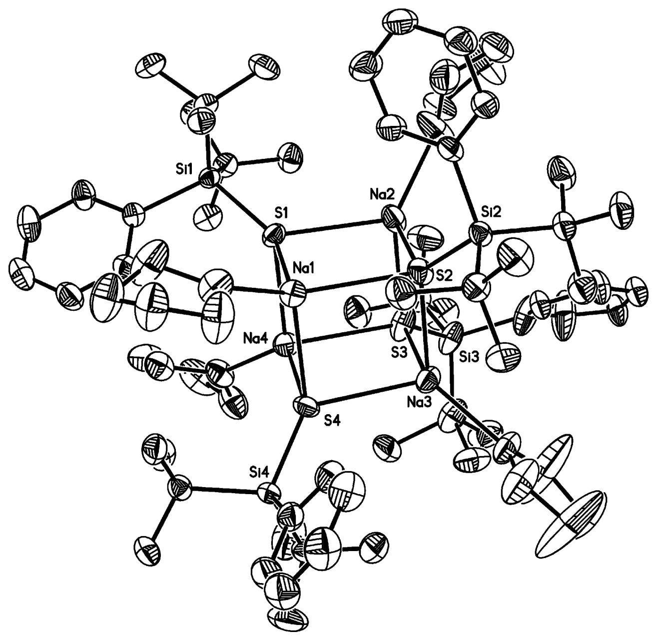

Figure 1. Solid-state structure of **1a**. Thermal ellipsoids are drawn at the 50% probability level. Hydrogen atoms have been omitted for clarity.

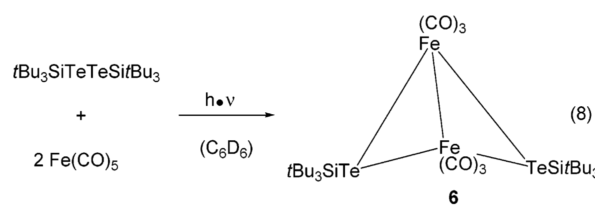

(8)

NMR Spectra. When considering the ^{1}H, ^{13}C, and ^{29}Si NMR spectra of the chalcogenols, dichalcogenides, and chalcogenolates, certain general trends can be observed. As is to be expected upon the replacement of an alkyl group with an aryl substituent, the signals of all nuclei are shifted downfield in the ${}^t\mathrm{Bu_3Si^-}$ compounds as compared to the corresponding compounds with $t\mathrm{Bu_2PhSi^-}$ substituents. In addition, the signals of the silicon atoms and the quaternary carbon atoms of the *tert*-butyl groups are shifted downfield as the chalcogen is changed from sulfur to selenium to tellurium. This effect can be observed among the dichalcogenides and chalcogenols, as well as among the chalcogenolates. It is always more pronounced for the ^{29}Si signals than for the quaternary ^{13}C signals, and the relative difference in chemical shift is generally larger between sulfur and selenium than it is between selenium and tellurium. The aromatic and alkyl proton signals and the signals of the primary ^{13}C atoms also tend to be shifted downfield in compounds containing the heavier chalcogens, but the change in chemical shift is smaller, making such trends more difficult to discern. No general trend can be applied to the relative shifts of any nucleus when comparing an analogous chalcogenolate, dichalcogenide, and chalcogenol (i.e., **1a**, **2a**, and **3a**). Among the six chalcogenols, **3a**−**3f**, the signals of the

(8) For example: (a) Dey, S.; Kumbahare, L. B.; Jain, V. K.; Schurr, T.; Kaim, W.; Klein, A.; Belaj, F. *Eur. J. Inorg. Chem.* **2004**, 4510. (b) Liaw, W.-F.; Lee, J.-H.; Gau, H.-B.; Chen, C.-H.; Lee, G.-H. *Inorg. Chim. Acta* **2001**, *322*, 99. (c) Liaw, W.-F.; Chiang, M.-H.; Liu, C.-J.; Harn, P.-J. *Inorg. Chem.* **1993**, *32*, 1536. (d) Albano, V. G.; Monari, M.; Orabona, I.; Panunzi, A.; Ruffo, F. *J. Am. Chem. Soc.* **2001**, *123*, 4352.

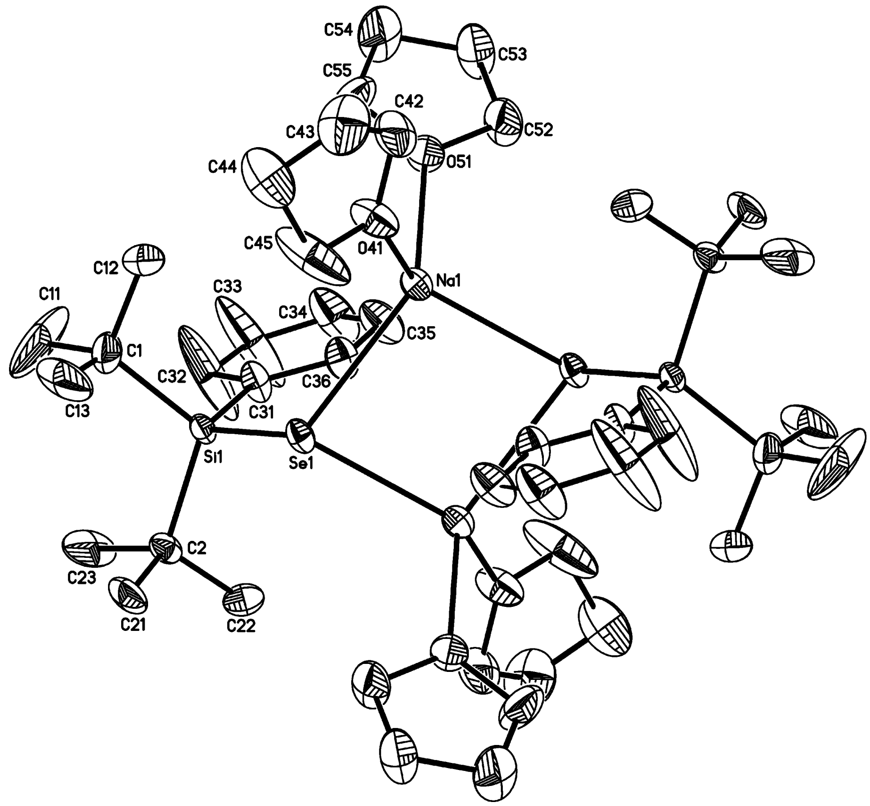

Figure 2. Solid-state structure of **1b**. Thermal ellipsoids are drawn at the 50% probability level. Hydrogen atoms have been omitted for clarity.

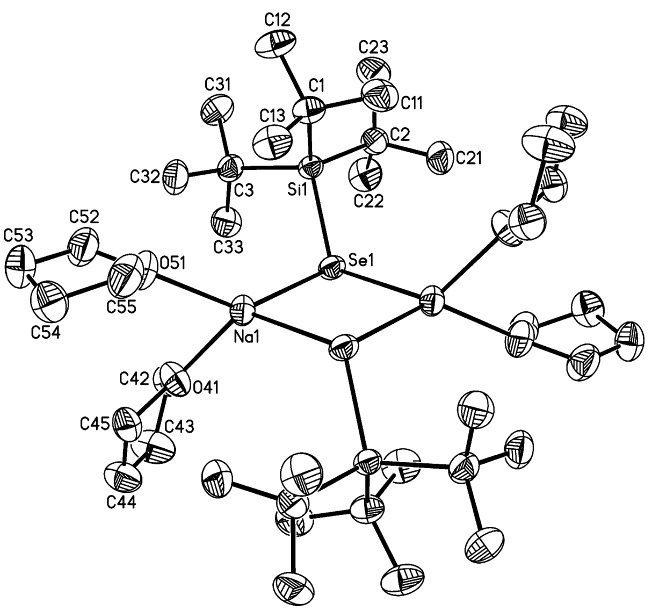

Figure 3. Solid-state structure of **1e**. Thermal ellipsoids are drawn at the 50% probability level. Hydrogen atoms have been omitted for clarity.

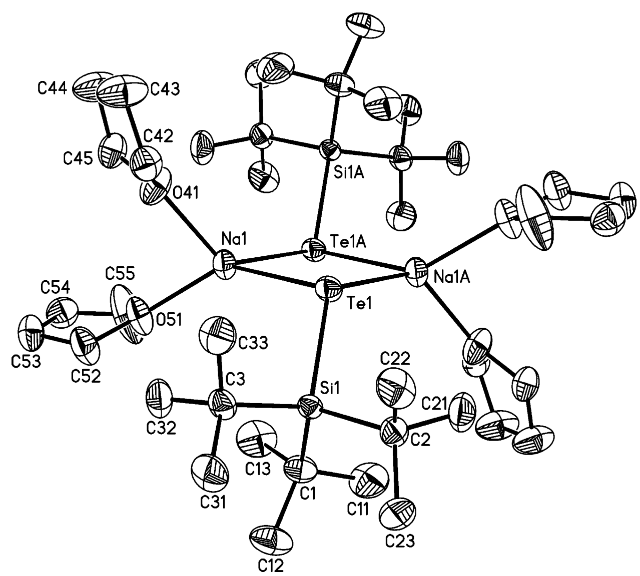

Figure 4. Solid-state structure of **1f**. Thermal ellipsoids are drawn at the 50% probability level. Hydrogen atoms have been omitted for clarity.

chalcogenolic protons, as mentioned above, display a pronounced upfield shift.

X-ray Crystallographic Structures. The molecular structures of chalcogenolates **1a**, **1b**, **1e**, **1f**, **4**, **5**, and **6** and dichalcogenides **2c** and **2f** are shown in Figures 1−9. Selected bond lengths and angles are listed in the corresponding figure captions and in Tables 1 and 2. Crystal data and refinement details are given in Tables 3−5.

Figure 1 represents the molecular structure of the sodium chalcogenolate $[(THF)NaSSiPh^{t}Bu_2]_4$ **1a** (monoclinic, $P2_1/n$; selected bond lengths and angles are in Table 1). In contrast to the core of the homologous siloxide $NaOSiPh^{t}Bu_2$,[9] the central core of **1a** possesses an almost regular heterocubane structure. The corners of this cube are alternately occupied by S and Na atoms [**1a**: S−Na−S (av) = 92.21(6)°, Na−S−Na (av) = 87.71(6)°]. In $NaSSiPh^{t}Bu_2$, no significant variations of the S−Si bond lengths are observed [**1a**: S−Si (av) = 2.8046(17) Å]. The coordination spheres of the alkali metals are completed by solvent

(9) Lerner, H.-W.; Scholz, S.; Bolte, M. *Organometallics* **2002**, *21*, 3827.

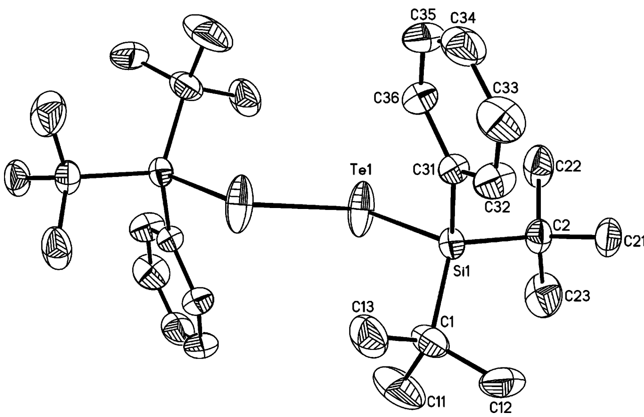

Figure 5. Solid-state structure of **2c**. Thermal ellipsoids are drawn at the 50% probability level. Hydrogen atoms have been omitted for clarity. The structures of **2a** and **2b** are analogous to that of **2c**.

molecules. Along with the three S atoms, each Na atom in **1a** is also coordinated by one molecule of tetrahydrofuran.

In contrast to the tetrameric solid-state structures of the unsolvated siloxides NaOSiR^{t}Bu$_2$ (R = ^{t}Bu, Ph)[9] and the monosolvated thiolate (THF)NaSSiPh^{t}Bu$_2$ **1a**, the central frameworks of the disolvated sodium chalcogenolates (THF)$_2$NaESi^{t}Bu$_3$ (E = O, Se, Te)[9] and (THF)$_2$NaSeSiPh^{t}Bu$_2$ are dimeric, forming four-membered rings. This structural motif is also observed for (THF)$_2$LiTeSi(SiMe$_3$)$_3$[5a] and for several arylsodium thiolates.[10] The molecular structures of **1b**, **1e**, and **1f** are shown in Figures 2−4 (selected bond lengths and angles are in Table 1). These sodium chalcogenolates crystallize in the space group $P2_1/n$, and their unit cells each contain two formula units. The sodium atoms in **1b**, **1e**, and **1f** are each coordinated by two chalcogen atoms and two tetrahydrofuran molecules in a distorted tetrahedral fashion.

The distances of 2.228(4) and 2.2364(6) Å in **1b** and **1e** are of a characteristic length for Se−Si bonds (the mean length of metal-bound Se−Si bonds is 2.283 Å).

X-ray quality crystals of **2a**−**2c**, **2e**, and **2f** were grown from pentane. Because **2a** and **2b** are isomorphous to **2c** and **2e** is isomorphous to **2f**, only the ditellurides are depicted (Figures 5 and 6). Selected bond lengths and angles for all of the structurally characterized dichalcogenides can be found in Table 2. Diselenide **2e** crystallizes in the trigonal space group $R\bar{3}$ with two independent molecules in the asymmetric unit. In the first molecule, the selenium atoms are disordered over two positions. The position of atom Se(1) is occupied to 76%; atom Se(1)′ is occupied to 24%. The corresponding atoms Se(1)#1 and Se(1)′#1 are generated by the crystallographic inversion center located in the center of the Se−Se bond. In the second molecule in the asymmetric unit, the silicon atoms (which are again related by a crystallographic inversion center) lie on a 3-fold rotational axis. This creates three positions for each selenium atom, each of which is occupied to $^1/_3$.

In the solid state, the dichalcogenides **2a** (monoclinic, $P2_1/n$), **2b** (monoclinic, $P2_1/c$), **2c** (monoclinic, $P2_1/c$), **2e** (both molecules), and **2f** (orthorhombic, *Pbca*) all possess Si−E−E−Si chains that are exactly trans. The corresponding torsional angles of 180° are mandated by the crystallographic inversion center located in the middle of each of the E−E bonds. These silyl dichalcogenides display Si−E−E angles smaller than 109° [**2a**, 108.08(3)°; **2b**, 100.238(19)°; **2c**, 98.22(2)°; **2e** (av), 99.5(4)°; **2f**, 103.03(3)°]. The S−S bond [2.0932(9) Å] in **2a** is somewhat longer than the typical bond lengths for aryl- and alkyl-substituted disulfides RS−SR (the mean S−S distance for aryl disulfides is 2.050 Å; the mean for alkyl disulfides is 2.024 Å).[17] The Se−Se and Te−Te bonds in dichalcogenides **2b**, **2c**, **2e**, and **2f**, however, have bond lengths similar to those found in the corresponding alkyl- and aryl-substituted dichalcogenides (**2b**, 2.3666(5) Å; **2e** (av), 2.360(2) Å; **2c**, 2.7243(3) Å; **2f**, 2.7398(7) Å; the mean Se−Se bond length for aryl diselenides is 2.347 Å, and for alkyl diselenides, it is 2.310; the mean Te−Te bond length for alkyl ditellurides is 2.724 Å).[17]

Tetrameric copper silyl thiolate **4**, shown in Figure 7, crystallizes in the tetragonal $I\bar{4}$ space group. The four copper atoms form a planar square with the thiolate ligands bridging pairs of adjacent copper atoms. The S−Cu−S angles, at 178.38(4)°, deviate slightly from linearity, whereas the Cu−S bond lengths, which average 2.16 Å, are typical for bridging thiolates. The Cu···Cu distances are quite short [2.8612(7) and 2.8613(7) Å], suggesting the possibility of bonding interactions between the metal centers. Similar structural motifs, including short M···M distances, have been observed for other silyl thiolate complexes of coinage metals.[1bc,11] The related complexes [Cu(SSiPh$_3$)]$_4$[1b] and [Cu(SSiMe$_2{}^t$Bu)]$_4$[1c] both display the central Cu$_4$S$_4$ eight-membered ring, although in these complexes, there are two shorter Cu···Cu interactions [2.852(1) Å and 2.8128(6) and 2.7413(7) Å, respectively] and two longer ones [3.027(1) Å and 2.9680(9) and 2.9541-(9) Å, respectively], rather than four contacts of the same

(10) For example: (a) Knotter, D. M.; Janssen, M. D.; Grove, D. M.; Smeets, W. J. J.; Horn, E.; Spek, A. L.; van Koten, B. *Inorg. Chem.* **1991**, *30*, 4361. (b) Olmstead, M. M.; Power, P. P.; Shoner, S. C. *J. Am. Chem. Soc.* **1991**, *113*, 3379. (c) Bochmann, M.; Bwernbya, G.; Grinter, R.; Lu, J.; Webb, K. J.; Williamson, W. J. *Inorg. Chem.* **1993**, *32*, 532. (d) Malik, M. A.; Motevalli, M.; Walsh, J. R.; O'Brian, P.; Jones, A. C. *J. Mater. Chem.* **1995**, *5*, 731.

(11) Wörner, A.; Polborn, K.; Wiberg, N.; Lerner, H.-W. CCDC 254421. Crystal data for [AgSSi^{t}Bu$_3$]$_4$: C$_{48}$H$_{108}$Ag$_4$Si$_4$, orthorhombic, space group $Cmc2_1$, a = 24.720(11) Å, b = 16.886(5) Å, c = 15.128(12) Å, α = 90°, β = 90°, γ = 90°; for preparation, see ref 12.

(12) Wörner, A. Ph.D. Thesis, University of Munich, Germany, 1998.

(13) (a) Englich, U.; Chadwick, S.; Ruhlandt-Senge, K. *Inorg. Chem.* **1998**, *37*, 283. (b) Chadwick, S.; Ruhlandt-Senge, K. *Chem.*−*Eur. J.* **1993**, *32*, 1536. (c) Niemeyer, M.; Power, P. P. *Inorg. Chem.* **1996**, *35*, 7264. (d) Rose, D. J.; Chang, D. Y.; Chen, Q.; Kettler, P. B.; Zubieta, J. *Inorg. Chem.* **1995**, *34*, 3973. (e) Anjali, K. S.; Vittal, J. J. *Main Group Met. Chem.* **2001**, *24*, 129. (f) Brianso, M. C.; Brianso, J. L.; Gaete, W.; Ros, J.; Suner, C. *J. Chem. Soc., Dalton Trans.* **1981**, 852.

(14) (a) Mathur, P.; Reddy, V. D.; Das, K.; Sinha, U. C. *J. Organomet. Chem.* **1991**, *409*, 255. (b) Bachman, R. E.; Witmire, K. H. *Organometallics* **1993**, *12*, 1988. (c) Shieh, M.; Chen, P.-F.; Tsai, Y.-C.; Shieh, M.-H.; Peng, S.-M.; Lee, G.-H. *Inorg. Chem.* **1995**, *34*, 2251.

(15) Wiberg, N.; Amelunxen, K.; Lerner, H.-W.; Schuster, H.; Nöth, H.; Krossing, I.; Schmidt-Ameluxen, M.; Seifert, T. *J. Organomet. Chem.* **1997**, *524*, 1.

(16) Lerner, H.-W.; Scholz, S.; Bolte, M.; Wagner, M. *Z. Anorg. Allg. Chem.* **2004**, *630*, 443. (b) Lerner, H.-W.; Scholz, S.; Bolte, M. *Z. Anorg. Allg. Chem.* **2001**, *627*, 1638.

(17) (a) *Cambridge Structural Database*, Version 5.25 with three updates; Cambridge University: Cambridge, England, July 2004. (b) Allen, F. H. *Acta Crystallogr., Sect. B* **2002**, *B58*, 380.

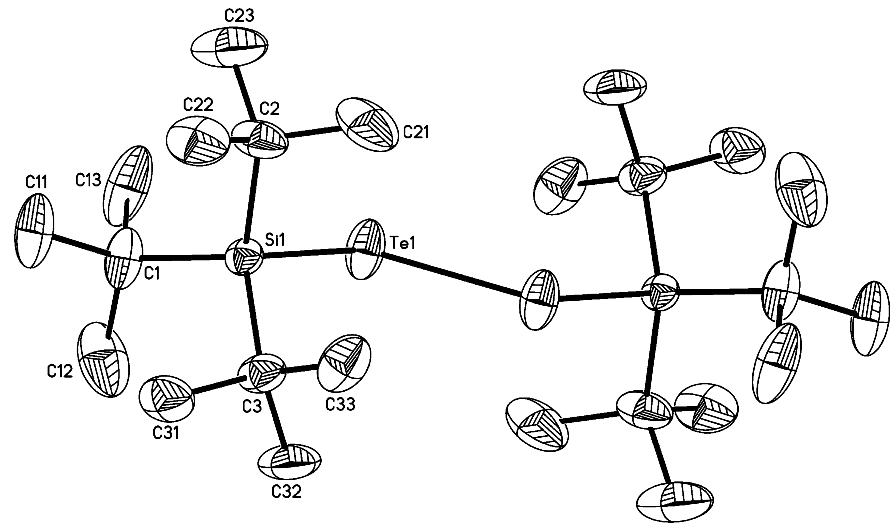

Figure 6. Solid-state structure of **2f**. Thermal ellipsoids are drawn at the 50% probability level. Hydrogen atoms have been omitted for clarity. The structure of **2e** is analogous to that of **2f**.

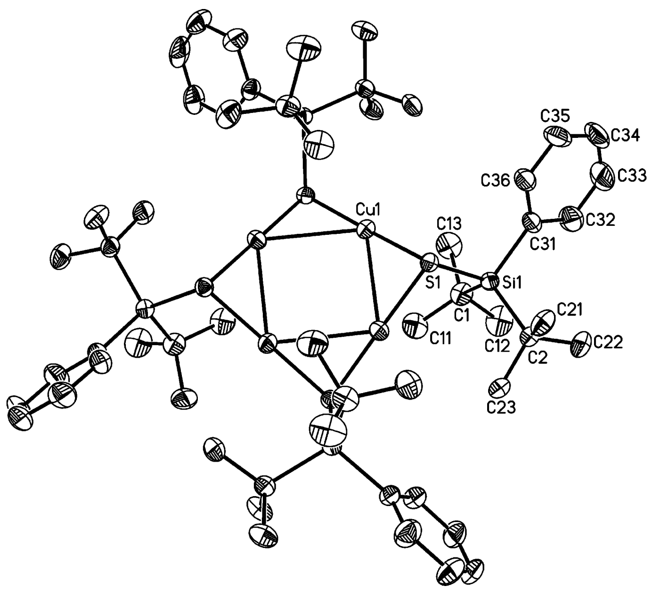

Figure 7. Solid-state structure of **4**. Thermal ellipsoids are drawn at the 50% probability level. Hydrogen atoms have been omitted for clarity. Selected bond lengths (Å) and angles (deg): S(1)−Si(1) = 2.1727(14), Si(1)−C(31) = 1.895(4), C−S (av) = 2.1597(10), Cu···Cu (av) = 2.8613(7), Si−C_{tBu} (av) = 1.924(5), S(1)−Cu(1)−S(1)#1 = 178.38(4), Cu(1)#2−Cu(1)−Cu(1)#1 = 89.984, Cu(1)−S(1)−Cu(1)#2 = 82.97(4), Cu(1)−S(1)−Si(1) = 108.85(5), Cu(1)#2−S(1)−Si(1) = 104.77. Symmetry transformations used to generate equivalent atoms: #1= $-y + {}^1/_2, x + {}^1/_2, -z + {}^3/_2$; #2 = $y - {}^1/_2, -x + {}^1/_2, -z + {}^3/_2$.

length, as seen in **4**. The silver thiolate $[AgSSi^tBu_3]_4$,[11] on the other hand, also displays four equal M···M distances (3.08 Å).

The zinc silyl thiolate **5** (monoclinic, *C*2/*c*), shown in Figure 8 (selected bond lengths and angles are in the figure caption), crystallizes with one complete and two half molecules in the asymmetric unit. The two half molecules are both related to their second halves (which are found in neighboring asymmetric units) via a 2-fold rotational axis. The structure displays a dimer with a central Zn_2S_2 ring. The tetrahedrally coordinated zinc atoms are bridged by the two thiolato ligands. Terminal *cis*-chloro and *cis*-THF ligands complete the coordination spheres. The coordination spheres of the zinc atoms are distorted; the Cl−Zn−S angles [127.47(7)−130.04(7)°] are widened considerably, whereas the S−Zn−S angles [88.18(6)−88.54(8)°] are quite small. The Zn−ligand distances vary only slightly between the four zinc atoms in the asymmetric unit, and all bond lengths are in the expected ranges. Such dimeric structures for thiolato-bridged zinc chloride complexes are unusual. However, several homoleptic zinc aryl thiolates also feature Zn_2S_2 rings in the solid state.[13a−d] The only structurally characterized complexes featuring Zn_2S_2 rings with terminal chloro ligands are anionic and display dichloro zinc moieties.[13e,f]

Iron carbonyl tellurolate **6** (monoclinic, *C*2/*c*), shown in Figure 9 (selected bond lengths and angles are in the figure caption), displays a butterfly geometry in the solid state. The iron and tellurium atoms sit at the corners of a slightly distorted tetrahedron. Each iron atom is coordinated by three carbonyl ligands. The distorted octahedral coordination spheres are completed by bonds to the two bridging tellurolate ligands and an iron−iron bond. This structural motif is found in other iron carbonyl tellurolates, although, to the best of our knowledge, no other similar complex with a silyl tellurolate exists.[14] The iron−iron distances in these complexes (2.605−2.657 Å) are in the same range as those in **6** [2.645(2) Å]. The Fe−Te distances, however, are somewhat shorter [the average is 2.54 Å vs 2.607(2) Å in **6**]. This disparity, however, can be attributed to the differences between the silyl substituent in **6** and the alkyl substituents in the other complexes.

Summary and Conclusion

In summary, it has been shown that the sodium silyl chalcogenolates $NaESiR^tBu_2$ (E = S, Se, Te; R = Ph, ^{t}Bu) can be prepared from precursor sodium silanides via chalcogen degradation. These chalcogenolates are sensitive to oxidation and protonolysis, yielding dichalcogenides and chalcogenols. The chalcogenolates and dichalcogenides have been studied by X-ray crystallography; all compounds have been characterized by proton and heteronucleus NMR spectroscopy.

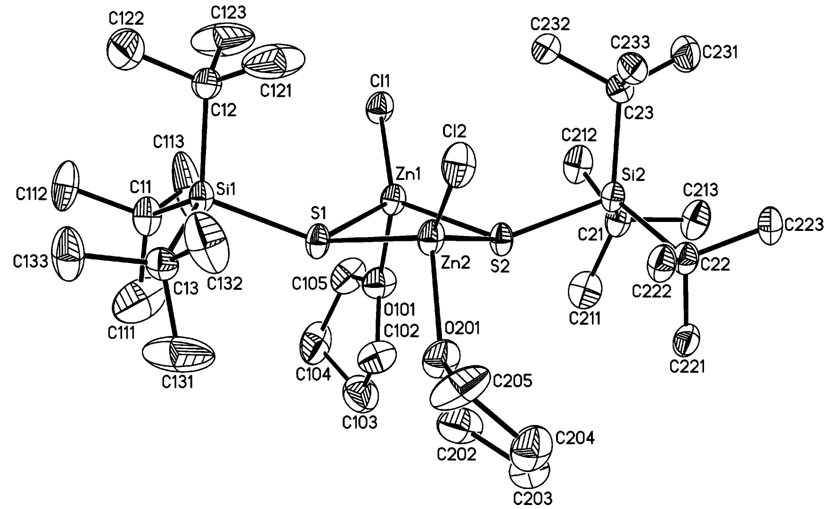

Figure 8. Solid-state structure of **5** (molecule a). Thermal ellipsoids are drawn at the 50% probability level. Hydrogen atoms have been omitted for clarity. Selected bond lengths (Å) and angles (deg). Molecule a: Zn−S (av) = 2.338(2), Zn−O (av) = 2.071(4), Zn−Cl (av) = 2.182(2), S−Si (av) = 2.162(2), Si−C (av) = 1.935(6), O−Zn−Cl (av) = 101.87(15), O−Zn−S (av) = 101.88(15), S−Zn−S (av) = 88.50(6), Zn−S−Zn (av) = 88.17(6), Si−S−Zn (av) = 126.35(8), Cl(1)−Zn(1)−S(2) = 129.07(7), Cl(1)−Zn(1)−S(1) = 130.04(7), Cl(2)−Zn(2)−S(1) = 129.33, Cl(2)−Zn(2)−S(2) = 127.47(7). Molecule b: Zn−S (av) = 2.336(2), Zn(3)−O(301) = 2.058(5), Zn(3)−Cl(3) = 2.184(2), S(3)−Si(3) = 2.167(3), Si−C (av) = 1.932(8), O(301)−Zn(3)−Cl(3) = 101.65(18), O−Zn−S (av) = 102.71(18), S(3)−Zn(3)−S(3)#1 = 88.41(7), Zn(3)−S(3)−Zn(3)#1 = 88.76(7), Si−S−Zn (av) = 126.41(10), Cl(3)−Zn(3)−S(3) = 129.62(9), Cl(3)−Zn(3)−S(3)#1 = 127.56(10). Molecule c: Zn−S (av) = 2.342(2), Zn(4)−O(401) = 2.057(5), Zn(4)−Cl(4) = 2.187(2), S(4)−Si(4) = 2.167(3), Si−C (av) = 1.929(7), O(401)−Zn(4)−Cl(4) = 102.35(18), O−Zn−S (av) = 101.8(2), S(4)−Zn(4)−S(4)#1 = 88.54(8), Zn(4)−S(4)−Zn(4)#1 = 87.68(7), Si−S−Zn (av) = 126.35(11), Cl(4)−Zn(4)−S(4) = 128.35(9), Cl(4)−Zn(4)−S(4)#1 = 129.19(9). Symmetry transformations used to generate equivalent atoms: #1 = $-x + 2, y, -z + {}^{3}/_{2}$.

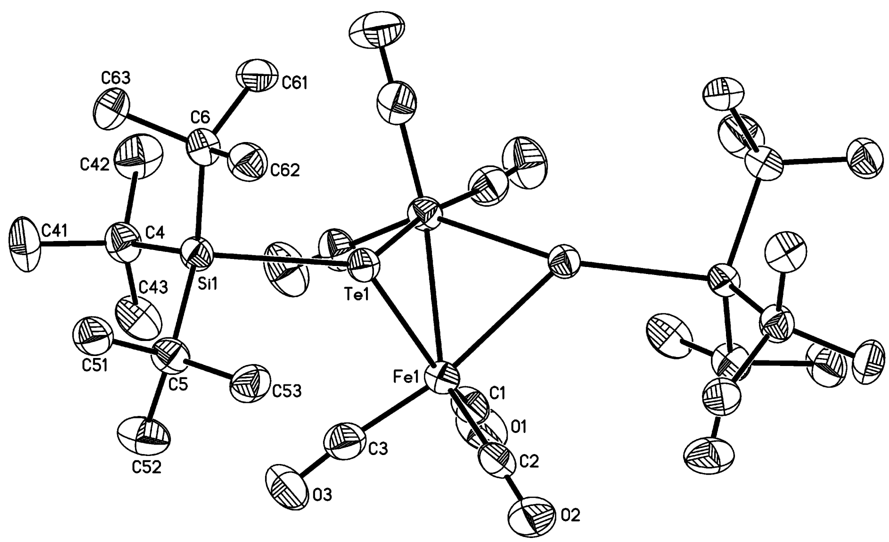

Figure 9. Solid-state structure of **6**. Thermal ellipsoids are drawn at the 50% probability level. Hydrogen atoms have been omitted for clarity. Selected bond lengths (Å) and angles (deg): Fe(1)−Fe(1)#1 = 2.645(2), Fe−C (av) = 1.784(9), C−O (av) = 1.138(11), Fe−Te (av) = 2.6074(11), Te(1)−Si(1) = 2.622(2), Si−C (av) = 1.945(8), Te−Fe−Fe (av) = 59.44(4), Fe(1)−Te(1)−Fe(1)#1 = 61.11(4), Te(1)−Fe(1)−Te(1)# = 177.04(3), Fe−Te−Si (av) = 125.33(5). Symmetry transformations used to generate equivalent atoms: #1 = $-x + 1, y, -z + {}^{1}/_{2}$.

The silyl chalcogenolates show promise as ligands for potentially redox-active transition metal clusters. The complexes $[Cu(SSiPh^tBu_2)]_4$, $[ZnCl(SSi^tBu_3)(THF)]_2$, and $[Fe(TeSi^tBu_3)(CO)_3]_2$ have been isolated and structurally characterized.

Experimental

General Considerations. All experiments were carried out under dry argon or nitrogen using standard Schlenk and glovebox techniques. Alkane solvents were dried over sodium and freshly distilled prior to use. THF and toluene were distilled from sodium/benzophenone. C_6D_6 was dried over molecular sieves and stored under dry nitrogen. $NaSi^tBu_3$[15] and $NaSiPh^tBu_2$[16] were prepared according to published procedures. All other starting materials were purchased from commercial sources and used without further purification. NMR spectra were recorded on Bruker AM 250, Bruker DPX 250, Bruker AMX 400, and Bruker Advance 400 spectrometers. The ^{29}Si spectra were recorded using the INEPT pulse sequence with empirically optimized parameters for polarization transfer from the *tert*-butyl substituents. Using $Te(OH)_6$ in D_2O at 712 ppm as an external standard, we referenced the ^{125}Te spectra to Me_2Te at 0 ppm. ^{77}Se spectra were referenced to Me_2Se at 0 ppm. IR spectra were recorded on a Perkin-Elmer 1650 FTIR spectrophotometer. Elemental analyses were performed at the microanalytical laboratories of the Universität Frankfurt. Cyclic

Table 1. Selected Bond Lengths [Å] and Angles [deg] for Chalcogenolates **1a**, **1b**, **1e**, and **1f**

	1a	**1b**	**1e**	**1f**
Si−E	2.0846(17) (av)	2.228(4)	2.2364(6)	2.4654(7)
E−Na	2.7664(30) (av)	2.881(6) (av)	2.8677(9) (av)	3.0617(12) (av)
Na−O	2.295(4) (av)	2.289(14) (av)	2.3092(18) (av)	2.287(3) (av)
Si−C_{tBu}	1.919(5) (av)	1.928(20) (av)	1.952(2) (av)	1.948(3) (av)
Si−C_{Ph}	1.894(5) (av)	1.873(14) (av)		
Si−E−Na	126.72(9) (av)	109.83(17) (av)	114.76(2) (av)	114.26(3) (av)
Na−E−Na	87.71(6) (av)	82.72(18)	83.01(2)	80.80(3)
E−Na−E	92.21(6) (av)	97.28(18)	96.99(2)	99.20(3)

Table 2. Selected Bond Lengths [Å] and Angles [deg] for Dichalcogenides **2a**−**2c**, **2e**, and **2f**

	2a	**2b**	**2c**	**2e**[a]	**2e**[a]	**2f**
E−E	2.0932(9)	2.3666(5)	2.7243(4)	2.332(19) (av)	2.388(10)	2.7398(7)
Si−E	2.1675(6)	2.3106(6)	2.5180(8)	2.414(7) (av)	2.421(10)	2.5517(12)
Si−C_{tBu}	1.9120(18) (av)	1.919(2) (av)	1.923(3) (av)	1.926(20) (av)	1.908(19)	1.933(6) (av)
Si−C_{Ph}	1.8840(17) (av)	1.884(2)	1.884(3)			
Si−E−E	102.08(3)	100.238(19)	98.22(2)	99.93(40) (av)	99.1(3)	103.03(3)
Si−E−E−Si	180	180	180	180	180	180

[a] Two independent molecules in the asymmetric unit.

Table 3. Crystal Data and Structure Refinement Parameters for **1a**, **1b**, **1e**, and **1f**

	1a	**1b**	**1e**	**1f**
empirical formula	$C_{72}H_{124}Na_4O_4S_4Si_4$	$C_{44}H_{78}Na_2O_4Se_2Si_2$	$C_{40}H_{86}Na_2O_4Se_2Si_2$	$C_{40}H_{86}Na_2O_4Se_2Si_2$
color	colorless	colorless	colorless	colorless
shape	block	block	block	block
fw	1386.27	931.14	891.17	988.45
cryst syst	monoclinic	monoclinic	monoclinic	monoclinic
space group	$P2_1/c$	$P2_1/n$	$P2_1/n$	$P2_1/n$
a, Å	21.3211(14)	10.1564(17)	8.9662(8)	9.0926(6)
b, Å	14.6608(9)	14.708(2)	15.6100(9)	16.5792(13)
c, Å	29.3525(18)	17.355(2)	17.4525(15)	17.0318(11)
α, deg	90	90	90	90
β, deg	90.022(5)	98.172(12)	90.224(7)	90.693(5)
γ, deg	90	90	90	90
vol (Å^3), Z	9174.8(10), 4	2566.2(2), 2	2442.7(3), 2	2567.3(3), 2
density (calcd), mg/m^3	1.004	1.205	1.212	1.279
abs coeff μ(Mo Kα), mm^{-1}	0.212	1.540	1.614	1.232
F(000)	3008	984	952	1024
cryst size, mm^3	0.52 × 0.46 × 0.33	0.42 × 0.38 × 0.35	0.34 × 0.28 × 0.22	0.36 × 0.26 × 0.20
reflns collected	49 292	24 241	25 568	28 074
independent reflns	16315	4531	4610	5006
final R indices [$I > 2\sigma(I)$], R1, wR2	0.0828, 0.2030	0.1691, 0.3697	0.0289, 0.0574	0.0263, 0.0606

Table 4. Crystal Data and Structure Refinement Parameters for **2a**, **2b**, **2c**, **2e**, and **2f**

	2a	**2b**	**2c**	**2e**	**2f**
empirical formula	$C_{28}H_{46}S_2Si_2$	$C_{28}H_{46}Se_2Si_2$	$C_{28}H_{46}Te_2Si_2$	$C_{24}H_{54}Se_2Si_2$	$C_{24}H_{54}Te_2Si_2$
color	yellow	red	blue	red	blue
shape	block	block	block	block	block
fw	502.95	596.75	694.03	556.77	654.05
cryst syst	monoclinic	monoclinic	monoclinic	trigonal	orthorhombic
space group	$P2_1/n$	$P2_1/c$	$P2_1/c$	$R\bar{3}$	$Pbca$
a, Å	8.7385(9)	8.2842(7)	8.2602(7)	20.188(2)	14.6569(16)
b, Å	14.8594(18)	14.9971(11)	15.3176(9)	20.188(2)	13.5911(17)
c, Å	11.8876(12)	12.4940(11)	12.8106(10)	25.220(3)	15.1033(16)
α, deg	90	90	90	90	90
β, deg	108.113(8)	105.242(7)	106.888(7)	90	90
γ, deg	90	90	90	120	90
vol (Å^3), Z	1467.1(3), 2	1497.6(2), 2	1561.1(2), 2	8901.5(16), 12	3008.6(6), 4
density (calcd), mg/m^3	1.139	1.323	1.476	1.264	1.444
abs coeff μ(Mo Kα), mm^{-1}	0.277	2.563	1.959	2.582	2.027
F(000)	548	620	692	3528	1320
cryst size, mm^3	0.19 × 0.15 × 0.09	0.32 × 0.24 × 0.16	0.39 × 0.32 × 0.26	0.36 × 0.32 × 0.28	0.13 × 0.13 × 0.13
reflns collected	13 328	22 434	23 713	12 998	15 595
independent reflns	2879	3083	4415	3537	2675
final R indices [$I > 2\sigma(I)$], R1, wR2	0.0327, 0.0719	0.0301, 0.0678	0.0387, 0.1030	0.1596, 0.3927	0.0366, 0.0616

voltammetry was performed on a Princeton Applied Research potentiostat in THF solution with $[NBu_4][PF_6]$ as the electrolyte. A platinum electrode was used with ferrocene as an internal standard. Mass spectrometry [electrospray ionization (ESI)] was performed with a Fisons VG Platform II instrument. UV−vis absorption spectroscopy was carried out in cyclohexane using a Varian Cary 50 Scan spectrophotometer and a Perkin-Elmer 555 spectrophotometer.

Table 5. Crystal Data and Structure Refinement Parameters for **4**, **5**, and **6**

	4	**5**	**6**
empirical formula	$C_{56}H_{92}Cu_4S_4Si_4$	$C_{32}H_{70}S_2Cl_2Zn_2O_2Si_2$	$C_{30}H_{54}Fe_2O_6Si_2Te_2$
color	colorless	orange	red
shape	needle	block	plate
fw	1260.06	808.82	933.81
cryst syst	tetragonal	monoclinic	monoclinic
space group	$I\bar{4}$	$C2/c$	$C2/c$
a, Å	20.106(2)	44.727(3)	15.975(2)
b, Å	20.106(2)	17.3710(9)	28.272(3)
c, Å	7.7980(8)	21.8803(13)	11.2282(16)
α, deg	90	90	90
β, deg	90	101.404(5)	131.151(9)
γ, deg	90	90	90
vol (Å^3), Z	3152.4(5), 2	16664.3(17), 16	3818.5(8), 4
density (calcd), mg/m^3	1.328	1.290	1.624
abs coeff μ(Mo Kα), mm^{-1}	1.573	1.463	2.356
F(000)	1328	6912	1864
cryst size, mm^3	0.38 × 0.08 × 0.06	0.42 × 0.35 × 0.28	0.24 × 0.20 × 0.06
reflns collected	9708	10 4097	14 814
independent reflns	2988	15 698	3583
final R indices [$I > 2\sigma(I)$], R1, wR2	0.0359, 0.0696	0.0631, 0.1664	0.0498, 0.1287

Synthesis of Sodium Silyl Chalcogenolates 1a−1f. A Schlenk flask is charged with 3 mmol of elemental chalcogen to which is added a solution of an equimolar amount of silanide in THF (10 mL). After 16 h at room temperature, the product is obtained in THF solution with ca. 5% impurity due to disilane, and the product is used without further purification. Slow evaporation of the solvent leads to the deposition of colorless crystals.

(THF)NaSSiPh^{t}Bu$_2$ (1a). ^{1}H NMR (C_6D_6): 8.251 (m, 2H, *m*-Ph), 7.302 (m, 3H, *o*/*p*-Ph), 3.401 (m, 4H, THF OC*H*$_2$), 1.291 (s, 18H, ^{t}Bu$_2$), 1.223 (m, 4H, THF CC*H*$_2$) ppm. ^{13}C NMR (C_6D_6): 141.9 (*o*-Ph), 136.8 (*m*-Ph), 127.0 (*p*-Ph), 68.0 (THF O*C*H$_2$), 29.8 [C(*C*H$_3$)$_3$], 25.5 (THF C*C*H$_2$), 19.0 (*C*Me$_3$) ppm. ^{29}Si NMR (C_6D_6): 19.4 ppm.

(THF)$_2$NaSeSiPh^{t}Bu$_2$ (1b). ^{1}H NMR (C_6D_6): 8.364 (m, 2H, *m*-Ph), 7.31 (m, 3H, *o*/*p*-Ph), 3.435 (m, 8H, THF OC*H*$_2$), 1.350 (s, 27H, ^{t}Bu$_2$), 1.191 (m, 8H, THF CC*H*$_2$) ppm. ^{13}C NMR (C_6D_6): 141.0 (*o*-Ph), 137.2 (*m*-Ph), 127.0 (*p*-Ph), 68.0 (THF O*C*H$_2$), 30.2 [C(*C*H$_3$)$_3$], 25.5 (THF C*C*H$_2$), 19.1 (*C*Me$_3$) ppm. ^{29}Si NMR (C_6D_6): 25.9 ppm.

(THF)$_2$NaTeSiPh^{t}Bu$_2$ (1c). ^{1}H NMR (C_6D_6): 8.470 (m, 2H, *m*-Ph), 7.325 (m, 3H, *o*/*p*-Ph), 3.524 (m, 8H, THF OC*H*$_2$), 1.442 (s, 18H, ^{t}Bu$_2$), 1.304 (m, 8H, THF CC*H*$_2$) ppm. ^{13}C NMR (C_6D_6): 139.9 (*o*-Ph), 138.2 (*m*-Ph), 127.1 (*p*-Ph), 68.1 (THF O*C*H$_2$), 30.8 [C(*C*H$_3$)$_3$], 25.5 (THF C*C*H$_2$), 22.0 (*C*Me$_3$) ppm. ^{29}Si NMR (C_6D_6): 29.4 ppm. ^{125}Te NMR (C_6D_6): −1457 ppm.

(THF)$_2$NaSSi^{t}Bu$_3$ (1d). ^{1}H NMR (C_6D_6): 3.60 (m, 8H, THF OC*H*$_2$), 1.42 (m, 8H, THF CC*H*$_2$), 1.359 (s, 27H, ^{t}Bu$_3$) ppm. ^{13}C NMR (C_6D_6): 68.0 (THF O*C*H$_2$), 31.5 [C(*C*H$_3$)$_3$], 25.3 (THF C*C*H$_2$), 24.3 (*C*Me$_3$) ppm. ^{29}Si NMR (C_6D_6): 25.5 ppm.

(THF)$_2$NaSeSi^{t}Bu$_3$ (1e). ^{1}H NMR (C_6D_6): 3.61 (m, 8H, THF OC*H*$_2$), 1.42 (m, 8H, THF CC*H*$_2$), 1.384 (s, 27H, ^{t}Bu$_3$) ppm. ^{13}C NMR (C_6D_6): 68.0 (THF O*C*H$_2$), 31.7 [C(*C*H$_3$)$_3$], 25.5 (THF C*C*H$_2$), 24.2 (*C*Me$_3$) ppm. ^{29}Si NMR (C_6D_6): 33.2 ppm. ^{77}Se NMR (C_6D_6): 133.6 ppm.

(THF)$_2$NaTeSi^{t}Bu$_3$ (1f). ^{1}H NMR (C_6D_6): 3.58 (m, 8H, THF OC*H*$_2$), 1.436 (s, 27H, ^{t}Bu$_3$), 1.41 (m, 8H, THF CC*H*$_2$) ppm. ^{13}C NMR (C_6D_6): 67.8 (THF O*C*H$_2$), 32.2 [C(*C*H$_3$)$_3$], 25.4 (THF C*C*H$_2$), 24.0 (*C*Me$_3$) ppm. ^{29}Si NMR (C_6D_6): 33.7 ppm.

Synthesis of Potassium Silyl Tellurolate KTeSi^{t}Bu$_3$. Ditelluride **2f** (20 mg, 0.03 mmol) and potassium metal (20 mg, 0.5 mmol) are combined in THF (0.6 mL). After 24 h at room temperature, the color has changed from blue to colorless. ^{1}H NMR (THF−d$_8$): 1.187 (s, 27H, ^{t}Bu$_3$) ppm. ^{13}C NMR (C_6D_6): 32.89 [C(*C*H$_3$)$_3$], 24.10 (*C*Me$_3$) ppm. ^{29}Si NMR (C_6D_6): 31.8 ppm.

Synthesis of Disilyldichalcogenides 2a−2f. Air oxidation of THF solutions of the sodium silyl chalcogenolates yields the corresponding disilyldichalogenides quantitatively, as determined by NMR spectroscopy. These compounds can be freed of byproduct salts by removal of the THF solvent, extraction with pentane, and filtration.

Alternate Method for Preparation of Disulfides ^{t}Bu$_3$SiSSSi^{t}Bu$_3$ and ^{t}Bu$_2$PhSiSSSiPh^{t}Bu$_2$. To a stirring solution of sodium silanide (1.0 mmol) in 5 mL of THF is added 0.5 mmol of S_2Cl_2. After 1 h, the solvent is removed and the residue extracted with pentane. Filtration and concentration of the filtrate yields the product as a pale yellow solid.

^{t}Bu$_2$PhSiSSSiPh^{t}Bu$_2$ (2a). Recrystallization from pentane at 4 °C yields the product as pale yellow blocks. ^{1}H NMR (C_6D_6): 7.777 (m, 4H, *m*-Ph), 7.174 (m, 6H, *o*/*p*-Ph), 1.078 (s, 36H, ^{t}Bu$_2$) ppm. ^{13}C NMR (C_6D_6): 135.7 (*o*-Ph), 129.6 (*m*-Ph), 129.1 (*p*-Ph), 28.8 [C(*C*H$_3$)$_3$], 21.6 (*C*Me$_3$) ppm. ^{29}Si NMR (C_6D_6): 23.1 ppm. MS (ESI) *m*/*z*: 251 (100%, ^{t}Bu$_4$Ph$_2$Si$_2$S$_2$$^{2-}$). Elem Anal. Calcd for $C_{28}H_{46}S_2Si_2$: C, 66.86; H, 9.22%. Found: C, 64.66; H, 9.42%.

^{t}Bu$_2$PhSiSeSeSiPh^{t}Bu$_2$ (2b). Red blocks of the product can be obtained by recrystallization from pentane. ^{1}H NMR (C_6D_6): 8.081 (m, 4H, *m*-Ph), 7.232 (m, 6H, *o*/*p*-Ph), 1.277 (s, 36H, ^{t}Bu$_2$) ppm. ^{13}C NMR (C_6D_6): 136.9 (*o*-Ph), 133.2 (*m*-Ph), 127.9 (*p*-Ph), 30.2 [C(*C*H$_3$)$_3$], 23.9 (*C*Me$_3$) ppm. ^{29}Si NMR (C_6D_6): 26.5 ppm. MS (ESI) *m*/*z*: 299 (100%, ^{t}Bu$_4$Ph$_2$Si$_2$Se$_2$$^{2-}$, correct isotope pattern), 163 (52%, ^{t}BuPhSi$^-$). Elem Anal. Calcd for $C_{28}H_{46}Se_2Si_2$: C, 56.35; H, 7.77%. Found: C, 56.10; H, 7.70%. UV−vis λ_{max}: 424 nm.

^{t}Bu$_2$PhSiTeTeSiPh^{t}Bu$_2$ (2c). Recrystallization from pentane yields the product as dark blue blocks. ^{1}H NMR (C_6D_6): 8.071 (m, 4H, *m*-Ph), 7.227 (m, 6H, *o*/*p*-Ph), 1.273 (s, 36H, ^{t}Bu$_2$) ppm. ^{13}C NMR (C_6D_6): 137.7 (*o*-Ph), 134.7 (*m*-Ph), 129.7 (*p*-Ph), 30.5 [C(*C*H$_3$)$_3$], 24.0 (*C*Me$_3$) ppm. ^{29}Si NMR (C_6D_6): 26.5 ppm. MS (ESI) *m*/*z*: 349 (20%, ^{t}Bu$_4$Ph$_2$Si$_2$Te$_2$$^{2-}$, correct isotope pattern), 269 (33%, Ph^{t}BuSiTe$^-$), 235 (100%, Ph^{t}Bu$_2$SiO$^-$), 163 (17%, ^{t}BuPhSi$^-$).

^{t}Bu$_3$SiSSSi^{t}Bu$_3$ (2d). ^{1}H NMR (C_6D_6): 1.314 (s, 54H, ^{t}Bu$_3$) ppm. ^{13}C NMR (C_6D_6): 30.9 [C(*C*H$_3$)$_3$], 25.4 (*C*Me$_3$) ppm. ^{29}Si NMR (C_6D_6): 25.1 ppm. MS (ESI) *m*/*z*: 351 (14%, ^{t}Bu$_4$Si$_2$S$_2$$^-$), 263 (21%, ^{t}Bu$_3SiS_2$$^-$), 231 (100%, ^{t}Bu$_6Si_2S_2$$^{2-}$), 163 (48%). Elem Anal. Calcd for $C_{24}H_{54}S_2Si_2$: C, 62.26; H, 11.76%. Found: C, 59.64; H, 11.63%.

^{t}Bu$_3$SiSeSeSi^{t}Bu$_3$ (2e). The diselenide can be obtained as brick-red blocks by recrystallization from pentane. ^{1}H NMR (C_6D_6): 1.316 (s, 54H, ^{t}Bu$_3$) ppm. ^{13}C NMR (C_6D_6): 31.0 [C(CH$_3$)$_3$], 26.3 (CMe$_3$) ppm. ^{29}Si NMR (C_6D_6): 30.7 ppm. ^{77}Se NMR (C_6D_6): −82.3 ($^1J_{^{77}\mathrm{SeSi}}$ = 136.12 Hz) ppm. MS (ESI) m/z: 279 (100%, ^{t}Bu$_6$Si$_2$Se$_2^{2-}$, correct isotope pattern), 215 (80%, $Si_2Se_2^-$). Elem Anal. Calcd for $C_{24}H_{54}Se_2Si_2$: C, 51.77; H, 9.78%. Found: C, 47.44; H, 9.11%. UV−vis λ_{max}: 418 nm.

^{t}Bu$_3$SiTeTeSi^{t}Bu$_3$ (2f). Recrystallization from pentane results in the deposition of large, ink-blue plates of ditelluride. ^{1}H NMR (C_6D_6): 1.308 (s, 54H, ^{t}Bu$_3$) ppm. ^{13}C NMR (C_6D_6): 31.5 [C(CH$_3$)$_3$], 26.3 (CMe$_3$) ppm. ^{29}Si NMR (C_6D_6): 33.8 ppm. ^{125}Te NMR (C_6D_6): −624.2 ($^1J_{^{125}\mathrm{TeSi}}$ = 343.45 Hz) ppm. MS (ESI) m/z: 407 (50%), 335 (100%, ^{t}Bu$_6$Si$_2$OTe$_2^{2-}$, correct isotope pattern). Elem Anal. Calcd for $C_{24}H_{54}Te_2Si_2$: C, 44.07; H, 8.32%. Found: C, 44.12; H, 8.34%. UV−vis λ_{max}: 576, 292 nm.

Synthesis of Silyl Chalcogenols 3a−3f. The sodium silyl chalcogenolates are treated with an excess of trifluoroacetic acid in C_6D_6. Conversion is quantitative, as determined by NMR spectroscopy.

^{t}Bu$_2$PhSiSH (3a). ^{1}H NMR (C_6D_6): 7.803 (m, 2H, m-Ph), 7.160 (m, 3H, o/p-Ph), 1.059 (s, 18H, ^{t}Bu$_2$), −0.221 (s, 1H, SH) ppm. ^{13}C NMR (C_6D_6): 135.7 (o-Ph), 134.6 (m-Ph), 129.6 (p-Ph), 28.8 [C(CH$_3$)$_3$], 21.6 (CMe$_3$) ppm. ^{29}Si NMR (C_6D_6): 21.8 ppm.

^{t}Bu$_2$PhSiSeH (3b). ^{1}H NMR (C_6D_6): 7.834 (m, 2H, m-Ph), 7.140 (m, 3H, o/p-Ph), 1.095 (s, 18H, ^{t}Bu$_2$), −2.294 (s, 1H, SeH, $^1J_{^{77}\mathrm{SeH}}$ = 53.4 Hz) ppm. ^{13}C NMR (C_6D_6): 136.2 (o-Ph), 134.3 (m-Ph), 129.6 (p-Ph), 29.1 [C(CH$_3$)$_3$], 21.9 (CMe$_3$) ppm. ^{29}Si NMR (C_6D_6): 28.3 ppm. ^{77}Se NMR (C_6D_6): −413.8 ($^1J_{^{77}\mathrm{SeH}}$ = 53.4 Hz) ppm.

^{t}Bu$_2$PhSiTeH (3c). ^{1}H NMR (C_6D_6): 7.90 (m, 2H, m-Ph), 7.142 (m, 3H, o/p-Ph), 1.126 (s, 18H, ^{t}Bu$_2$), −7.478 (s, 1H, TeH, $^1J_{^{125}\mathrm{TeH}}$ = 25 Hz) ppm. ^{13}C NMR (C_6D_6): 137.0 (o-Ph), 134.1 (m-Ph), 129.6 (p-Ph), 29.5 [C(CH$_3$)$_3$], 22.2 (CMe$_3$) ppm. ^{29}Si NMR (C_6D_6): 34.4 ppm. ^{125}Te NMR (C_6D_6): −862.7 ($^1J_{^{125}\mathrm{TeH}}$ = 25 Hz) ppm.

^{t}Bu$_3$SiSH (3d). ^{1}H NMR (C_6D_6): 1.097 (s, 27H, ^{t}Bu$_3$), −0.556 (s, 1H, SH) ppm. ^{13}C NMR (C_6D_6): 30.3 [C(CH$_3$)$_3$], 23.7 (CMe$_3$) ppm. ^{29}Si NMR (C_6D_6): 27.8 ppm.

^{t}Bu$_3$SiSeH (3e). ^{1}H NMR (C_6D_6): 1.114 (s, 27H, ^{t}Bu$_3$), −2.677 (s, 1H, SeH, $^1J_{^{77}\mathrm{SeH}}$ = 52.6 Hz) ppm. ^{13}C NMR (C_6D_6): 30.5 [C(CH$_3$)$_3$], 24.0 (CMe$_3$) ppm. ^{29}Si NMR (C_6D_6): 34.8 ppm. ^{77}Se NMR (C_6D_6): −413.9 ($^1J_{^{77}\mathrm{SeH}}$ = 52.6 Hz) ppm.

^{t}Bu$_3$SiTeH (3f). ^{1}H NMR (C_6D_6): 1.118 (s, 27H, ^{t}Bu$_3$), −7.983 (s, 1H, TeH) ppm. ^{13}C NMR (C_6D_6): 31.0 [C(CH$_3$)$_3$], 24.1 (CMe$_3$) ppm. ^{29}Si NMR (C_6D_6): 42.4 ppm.

Complex Synthesis. [Cu(SSiPh^{t}Bu$_2$)]$_4$ (4). A solution of NaSSiPh^{t}Bu$_2$ (0.32 mmol) in 1 mL of THF is added dropwise to solid CuCl (40 mg, 0.32 mmol). The red-brown solution is stirred overnight. After removal of the solvent under reduced pressure, the residue is extracted with toluene and filtered. Slow evaporation of the solvent yields the product as crystalline colorless needles (37 mg, 0.029 mmol, 37%). ^{1}H NMR (C_6D_6): 8.095 (m, 2H, m-Ph), 7.229 (m, 3H, o/p-Ph), 1.337 (s, 18H, ^{t}Bu$_2$) ppm. ^{13}C NMR (C_6D_6): 137.8 (o-Ph), 129.3 (m-Ph), 127.9 (p-Ph), 30.2 [C(CH$_3$)$_3$], 23.0 (CMe$_3$) ppm. ^{29}Si NMR (C_6D_6): 23.1 ppm. Elem Anal. Calcd for $C_{56}H_{92}S_4Si_4Cu_4$: C, 53.38; H, 7.36%. Found: C, 53.31; H, 7.80%.

[ZnCl(SSi^{t}Bu$_3$)(THF)]$_2$ (5). A solution of NaSSi^{t}Bu$_3$ (1 mmol) in 2.5 mL of THF is added dropwise to solid $ZnCl_2$ (74 mg, 0.5 mmol). The orange solution is stirred overnight. After removal of the solvent under reduced pressure, the residue is extracted with toluene and filtered. Slow evaporation of the solvent yields the product as colorless crystalline blocks (130 mg, 0.16 mmol, 64%). ^{1}H NMR (C_6D_6): 3.745 (m, 8H, THF OCH_2), 1.390 (s, 54H, ^{t}Bu$_3$), 1.343 (m, 8H, THF CCH_2) ppm. ^{13}C NMR (C_6D_6): 137.7 (o-Ph), 134.7 (m-Ph), 129.7 (p-Ph), 30.9 [C(CH$_3$)$_3$], 25.3 (CMe$_3$) ppm. ^{29}Si NMR (C_6D_6): 34.0 ppm. Elem Anal. Calcd for $C_{32}H_{70}O_2S_2Si_2Cl_2Zn_2$: C, 47.52; H, 8.72%. Found: C, 46.22; H, 8.81%.

[Fe(TeSi^{t}Bu$_3$)(CO)$_3$]$_2$ (6). Ditelluride **2f** (17 mg, 0.025 mmol) and $Fe(CO)_5$ (10 mg, 0.05 mmol) are combined in C_6D_6. The blue solution is irradiated with a fluorescent light bulb for 8 h. An accompanying color change to red is observed. Conversion is quantitative, as determined by NMR spectroscopy. Slow evaporation of the solvent yields the product as blood-red plates. ^{1}H NMR (C_6D_6): 1.195 (s, 54H, ^{t}Bu$_3$) ppm. ^{13}C NMR (C_6D_6): 31.5 [C(CH$_3$)$_3$], 26.6 (CMe$_3$) ppm. ^{29}Si NMR (C_6D_6): 45.1 ppm. ^{125}Te NMR (C_6D_6): −1280 ppm. IR (KBr pellet, CO$^-$ absorptions): 2044.0 (vs), 2006.6 (vs), 1978.9 (s), 1963.0 (s), 1954.0 (s) cm^{-1}.

X-ray Structure Determination. Data collections were performed on a Stoe-IPDS-II two-circle diffractometer with graphite-monochromated Mo Kα radiation. The structures were solved with direct methods[18] and refined against F^2 by full-matrix least-squares calculations with SHELXL 97.[19] Hydrogen atoms were placed on ideal positions and refined with fixed isotropic displacement parameters using a riding model.

Acknowledgment. We are grateful to the University of Frankfurt for financial funding and Chemetall GmbH for a gift of *tert*-butyllithium.

Supporting Information Available: Table of X-ray parameters, atomic coordinates, and thermal parameters and bond distances and angles. This material is available free of charge via the Internet at http://pubs.acs.org.

IC048710J

(18) Sheldrick, G. M. *Acta Crystallogr., Sect. A* **1990**, *46*, 467.
(19) Sheldrick, G. M. *SHELXL 97*; University of Göttingen: Göttingen, Germany, 1997.